JES Focus Issue on Semiconductor Electrochemistry and Photoelectrochemistry in Honor of Krishnan Rajeshwar

Practical Aspects of Cyclic Voltammetry: How to Estimate Reduction Potentials When Irreversibility Prevails

Eli M. Espinoza,[1,=] John A. Clark,[2,=] Joey Soliman,[2] James B. Derr,[3] Maryann Morales,[1] and Valentine I. Vullev[1,2,3,4,z]

[1]*Department of Chemistry, University of California, Riverside, California 92521, USA*
[2]*Department of Bioengineering, University of California, Riverside, California 92521, USA*
[3]*Department of Biochemistry, University of California, Riverside, California 92521, USA*
[4]*Materials Science and Engineering Program, University of California, Riverside, California 92521, USA*

What is the best approach for estimating standard electrochemical potentials, $E^{(0)}$, from voltammograms that exhibit chemical irreversibility? The lifetimes of the oxidized or reduced forms of the majority of known redox species are considerably shorter than the voltammetry acquisition times, resulting in irreversibility and making the answer to this question of outmost importance. Half-wave potentials, $E^{(1/2)}$, provide the best experimentally obtainable representation of $E^{(0)}$. Due to irreversible oxidation or reduction, however, the lack of cathodic or anodic peaks in cyclic voltammograms renders $E^{(1/2)}$ unattainable. Therefore, we evaluate how closely alternative potentials, readily obtainable from irreversible voltammograms, estimate $E^{(0)}$. Our analysis reveals that, when $E^{(1/2)}$ is not available, inflection-point potentials provide the best characterization of redox couples. While peak potentials are the most extensively used descriptor for irreversible systems, they deviate significantly from $E^{(0)}$, especially at high scan rates. Even for partially irreversible systems, when the cathodic peak is not as pronounced as the anodic one, the half-wave potentials still provide the best estimates for $E^{(0)}$. The importance of these findings extends beyond the realm of electrochemistry and impacts fields, such as materials engineering, photonics, cell biology, solar energy engineering and neuroscience, where cyclic voltammetry is a key tool.
 [DOI: 10.1149/2.0241905jes]

Manuscript submitted November 15, 2018; revised manuscript received January 14, 2019. Published January 28, 2019. *This paper is part of the JES Focus Issue on Semiconductor Electrochemistry and Photoelectrochemistry in Honor of Krishnan Rajeshwar.*

Cyclic voltammetry (CV) is the hallmark of electrochemical analysis and it impacts on countless fields outside of chemistry, such as materials science, photonics, cell biology, neuroscience, electrical engineering and condensed-phase physics.[1–10] Voltammograms provide a wealth of information about the charge-transfer and mass-transport processes at the surfaces of the working electrodes.[11–15] The evolving voltammetry theories, based on Butler-Volmer and Marcus-Hush formalisms, reveal key mechanistic insights about these interfacial phenomena.[16–20]

Estimating standard electrochemical potentials ($E^{(0)}$) of oxidation and reduction encompasses one of the most widely spread uses of CV, which makes this technique popular. The strong correlation of $E^{(0)}$ with the energy levels of frontier orbitals and band edges defines the invaluable importance of the electrochemical potentials for characterization of electronic properties of molecular species and materials. Combining the Butler-Volmer equation with Fick's second law results in an expression of the faradaic current (i_F) in terms of the applied potential (E), where $E^{(0)}$ is one of the parameters. This expression of i_F as a function of E, however, is an integral equation and its solution remain in the realm of numerical analysis, rendering it impractical for routine estimations of $E^{(0)}$ from voltammograms. Therefore, half-wave potentials ($E^{(1/2)}$) have become the preferred representation of $E^{(0)}$, i.e., $E^{(1/2)} \approx E^{(0)}$ for reversible oxidation and reduction. The average between the anodic (E_a) and the cathodic (E_c) potentials define $E^{(1/2)}$, which are facile to extract from cyclic voltammograms manifesting reversibility (Figure 1a).[11] This definition of $E^{(1/2)}$ also extends to quasireversible cases (i.e., chemically reversible and electrochemically irreversible) when the rates of interfacial electron transfer are slower that the rates of mass transport to and away from the electrode and $|E_a - E_c|$ increases with an increase in the scan rate.[11,21]

The conundrum is how to estimate $E^{(0)}$ from voltammograms showing chemically irreversible oxidation and reduction (Figure 1b). Another question is how well $E^{(1/2)}$ estimates $E^{(0)}$ in the cases of partial chemical reversibility. For the rest of this discussion, we refer to "chemical reversibility" as "reversibility."

Chemical conversion, such as decomposition or dimerization, of the species produced on the electrode surface upon oxidation or reduction is the source of the observed chemical irreversibility. Two principal approaches allow for gaining reversibility: (1) increasing the scan rates so that the acquisition of the voltammograms is much faster than the lifetime of the formed oxidized or reduced species; and (2) lowering the temperature in order to slow down the undesired chemical conversions. The former approach produces voltammograms suffering from enormous capacitance currents (i_C) that are inherent for large scan rates. At scan rates of kV/s and MV/s, faradaic signals can be orders of magnitude smaller than the background, and decreasing the area of the working electrode, in order to decrease i_C, decreases the signal-to-noise ratios. Conversely, lowering the temperature sufficiently enough to attain reversibility limits the number of usable solvents with acceptable electrochemical windows due to their freezing points. Indeed, both of these approaches are quite involved, and they have not gained popularity as routine methods for electrochemical analysis.

When cyclic voltammograms show irreversible behavior, the most common practice involves reporting the peak potentials ($E^{(p)}$), i.e., anodic potentials (E_a) for oxidation or cathodic potentials (E_c) for reduction (Figure 1a). Voltammograms of reversible processes, however, elucidate that the values of the peak potentials deviate quite a bit from $E^{(1/2)}$, especially for large scan rates.

Another option involves the use of the edge potentials ($E^{(e)}$) of the anodic or cathodic waves as estimates of $E^{(0)}$ of irreversible processes (Figure 1). At the edges of the voltammogram waves, $E^{(e)}$ represents the potentials of the first detectable faradaic currents. Thus, $E^{(e)}$ underestimates $E^{(0)}$ of oxidation and overestimates $E^{(0)}$ of reduction by a few k_BT/F (k_BT is the thermal energy and F is the Faraday constant).

Conversely, we determined that the potentials, $E^{(i)}$ (Figure 1), at the inflection points of the anodic and cathodic waves are quite close to $E^{(1/2)}$ for reversible processes.[22] Therefore, we employ $E^{(i)}$ for estimating $E^{(0)}$ of irreversible oxidation and reduction.[23–27] Recently, Nicewicz et al. proposed the use of the half-peak potentials ($E^{(p/2)}$) for estimating $E^{(0)}$ of cyclic voltammograms showing irreversibility (Figure 1).[28] For symmetrical sigmoid curves progressing along the ordinate, the inflection points are at their half-heights, but the

[=]These authors contributed equally to this work.
[z]E-mail: vullev@ucr.edu

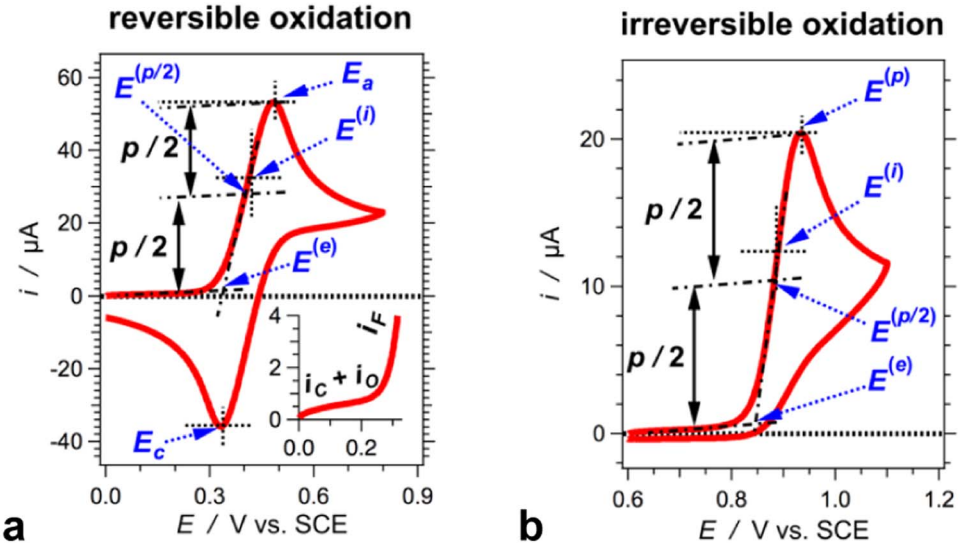

Figure 1. Examples of cyclic voltammograms showing chemically reversible and irreversible oxidation with designated potentials: E_a = anodic potential, E_c = cathodic potential, $E^{(i)}$ = inflection-point potential, $E^{(p/2)}$ = half-peak potential, $E^{(e)}$ = edge potential. (a) 1 mM ferrocene. Inset: the initiation of the scan showing the rise of the faradaic current, i_F, on the background of the capacitance current, i_C, and the ohmic current, i_O. (b) 1 mM 4Pip. (For both voltammograms: 200 mM $N(C_4H_9)_4PF_6$ in MeCN, and $v = 100$ mV s^{-1}.)

voltammogram waves do not necessary have such a shape leading to the peaks.

Herein, we review $E^{(1/2)}$, $E^{(i)}$, $E^{(p/2)}$, $E^{(p)}$, and $E^{(e)}$ extracted from cyclic voltammograms for reversible, irreversible and partially reversible electrochemical oxidation. ANOVA analysis[29] provides statistical quantification of how close the values of $E^{(i)}$, $E^{(p/2)}$, $E^{(p)}$, and $E^{(e)}$ are to those of $E^{(1/2)}$ for different scan rates. The values of $E^{(i)}$ are the closest to those of $E^{(1/2)}$, but $E^{(p/2)}$ fairs almost as well as $E^{(i)}$ in the statistical analysis. A straightforward differential analysis, i.e., the first and second derivatives of the cyclic voltammograms, provides convenient ways for determining peak potentials and inflection points. In addition, this differential approach proves immensely beneficial for estimating the reversibility of the electrochemical processes. Regression analysis reveals that even for partially reversible system, $E^{(1/2)}$ still provides a good estimate for $E^{(0)}$.

Experimental

Materials and general synthetic considerations.—All reagents and solvents were purchased from TCI America, Sigma-Aldrich and Alfa Aesar and used as received. The reaction progress was monitored by the means of thin layer chromatography (TLC), which was performed with aluminum foil plates, covered with silica gel 60 F254 (Merck). The products were purified using column chromatography packed with Kieselgel 60 (Merck). All reported ^{1}H-NMR and ^{13}C-NMR spectra were recorded on a 600 MHz spectrometer. Chemical shifts (δ/ppm) were determined using the solvent peaks as internal references. High-resolution mass spectra were obtained using electrospray MS (ESI-MS).

2-nitro-N-(tert-pentyl)-4-(piperidin-1-yl)benzamide (1).—2-Nitro-4-(piperidin-N-yl)-benzoic acid (1.0 g, 4 mmol), prepared as previously described,[30] was placed in a 100 mL Schlenk tube equipped with a magnetic stir bar. While purging with argon, chloro-*N*,*N*,*N*′,*N*′- tetramethylformamidinium hexafluorophosphate (2.0 g, 6 mmol) and 5 mL of dry dichloromethane (DCM) were added. The Schlenk tube was immersed in a dry ice/acetone bath and 2-methylbutan-2-amine (940 μL, 8 mmol) was slowly added to it followed by the addition of *N*-methylmorpholine (1.5 mL, 14 mmol). The reaction mixture was allowed to warm up to room temperature and was stirred overnight. The solution was diluted with 25 mL of DCM, and washed with 5% HCL (2 × 100 mL) and with a brine solution (100 mL). The organic layer was collected, dried over Na_2SO_4, and concentrated in vacuo. The product was purified using flash chromatography (column: 1" internal diameter, packed with silica gel in hexanes, 6" to 8" height of the packed stationary phase). The purification (stationary phase: silica gel; eluent gradient: from 100% hexanes to 100% ethyl acetate) afforded 1.01 g (3.17 mmol, 79% yield) of a yellow solid of **1**. ^{1}H NMR (600 MHz, $CDCl_3$) δ/ppm: 7.34 (1 H, d, $J = 2.56$ Hz), 7.30 (1 H, d, $J = 8.70$ Hz), 7.00 (1 H, d, $J = 7.68$ Hz), 5.43 (1 H, s), 3.27 (4 H, m), 1.79 (2 H, q, $J = 7.68$ Hz), 1.67 (4 H, m), 1.62 (2H, m), 1.37 (s, 1 H), 0.91 (3 H, t, $J = 7.42$ Hz). ^{13}C NMR (150 MHz, $CDCl_3$) δ/ppm: 165.87, 152.15, 148.25, 129.42, 122.43, 118.32, 109.84, 54.61, 49.22, 32.87, 26.19, 25.09, 24.00, 8.34. HRMS (*m/z*, ESI-TOF): calcd. for $C_{17}H_{26}N_3O_3^+$, 320.1974 $[M + H]^+$; found, 320.1956.

N-(tert-pentyl)-4-(piperidin-1-yl)-2-(2-propylpentanamido) benzamide (4Pip).—510 mg of **1** (1.6 mmol) and dicobalt octacarbonyl (1.1 g, 3.2 mmol) were placed in a 100 mL Schlenk tube equipped with a magnetic stir bar. While purging with argon, 5 mL of 1,2-dimethoxyethane and 2 drops of DI water were added. While stirring, the pressure tube was immersed in a temperature-controlled oil bath. The mixture was heated to 90°C and stirred for an hour. The reaction mixture was filtered; the filtrate was collected, diluted with 25 mL DCM, and washed with water (100 mL). The organic layer was collected, dried over Na_2SO_4, and concentrated in vacuo. The formed amine was used for the next step without further purification. While purging with argon, the resulting organic solid was transferred into a Schlenk tube using 5 mL dry DCM. The Schlenk tube was immersed in a dry ice/acetone bath, allowed to cool down, followed by addition of pivaloyl chloride (500 μL, 4 mmol) and *N*-methylmorpholine (750 μL, 6.8 mmol). The reaction mixture was allowed to warm up to room temperature and was stirred overnight. The solution was diluted with 25 mL of DCM, and washed with 5% HCL (2 × 100 mL) and with a brine solution (100 mL). The organic layer was collected, dried over Na_2SO_4, and concentrated in vacuo. The product was purified using flash chromatography (column: 1" internal diameter, was packed with silica gel in hexanes, 6" to 8" height of the packed stationary phase). The purification (stationary phase: silica gel: eluent gradient: from 100% hexanes to 100% ethyl acetate) afforded 435 mg, (1.2 mmol, 73% yield) of 4Pip. ^{1}H NMR (600 MHz, $CDCl_3$) δ/ppm: 11.51 (1 H, s), 8.29 (1 H, s), 7.21 (1 H, m), 6.47 (1 H, s), 5.68 (1 H, s), 3.27 (4 H, s), 1.80 (2 H, q, $J = 7.17$ Hz), 1.63 (4 H, s),

1.58 (2 H, s), 1.36 (6 H, s), 1.29 (10 H, s), 0.86 (3 H, t, $J = 7.42$ Hz). ^{13}C NMR (150 MHz, $CDCl_3$) δ/ppm: 178.04, 168.99, 153.96, 141.31, 127.35, 111.18, 108.33, 106.54, 54.38, 48.94, 40.18, 32.72, 27.59, 26.52, 25.38, 24.30, 8.39. HRMS (*m/z*, ESI-TOF): calcd. for $C_{22}H_{36}N_3O_3^+$, 390.2757 $[M + H]^+$; found, 374.2814.

2-nitro-N-(tert-pentyl)-5-(piperidin-1-yl)benzamide (2).—2-Nitro-5-(piperidin-*N*-yl)-benzoic acid (530 mg, 2.12 mmol), prepared as previously described,[31] was placed in a baked 50 mL round bottom flask equipped with a magnetic stir bar. While purging with argon, chloro-*N*,*N*,*N*′,*N*′-tetramethylformamidinium hexafluorophosphate (890 mg, 3.2 mmol) and 1,2-dichloroethane (5 mL) were added, and the reaction was cooled down in a dry ice/acetone bath. While stirring, 4-heptylamine (380 μL, 2.5 mmol) and 1 mL triethylamine (7.2 mmol) were slowly added. The reaction mixture was allowed to warm up to room temperature and was stirred overnight at 60°C. The solution was diluted with 25 mL of DCM, and washed with 5% HCL (2 × 100 mL) and with brine (100 mL). The organic layer was collected, dried over Na_2SO_4, and concentrated in vacuo. The product was purified using flash chromatography (column, 1″ internal diameter, packed with silica gel in hexanes, 6" to 8" height of the packed stationary phase). The purification (stationary phase: silica gel; eluent gradient: from 100% hexanes to 100% ethyl acetate) afforded 330 mg (0.95 mmol, 45% yield) of a yellow solid of **2**. ^{1}H NMR (600 MHz, $CDCl_3$) δ/ppm: 8.02 (1 H, d, $J = 9.2$ Hz), 6.77 (1 H, dd, $J = 9.5$, 2.8 Hz), 6.68 (1 H, d, $J = 3.1$ Hz), 5.39 (1 H, d, $J = 9.2$ Hz), 4.1 (1 H, m), 3.41 (4 H, m), 1.67 (6 H, m), 1.53 (2 H, m), 1.43 (6 H, m), 0.94 (6 H, t, $J = 7.2$ Hz). ^{13}C NMR (150 MHz, $CDCl_3$) δ/ppm: 167.43, 153.88, 136.47, 134.04, 127.43, 112.82, 112.16, 49.61, 48.43, 36.91, 25.18, 24.05, 19.03, 14.11. HRMS (*m/z*, ESI-TOF): calcd. for $C_{19}H_{30}N_3O_3^+$, 348.2287 $[M + H]^+$; found, 348.1938.

N-(heptan-4-yl)-5-(piperidin-1-yl)-2-(2-propylpentanamido) benzamide (5Pip).—290 of **2** (0.84 mmol) was suspended in ethyl acetate with 60 mg Pd/C (10%) in a 50 mL round bottom flask equipped with a magnetic stir bar. The mixture was stirred overnight under a hydrogen atmosphere at room temperature. The completion of the reduction led to a color change from yellow to colorless and appearance of blue fluorescence, which was monitored using TLC. The catalyst on the support was filtered out and the ethyl acetate was removed in vacuo. The solid was resuspended in 1,2-drichloroethane (5 mL), blanked with continuous flow of Ar and placed in a dry ice/acetone bath. Concurrently, 2-propylpentanoic acid (160 uL, 1 mmol) was converted to its acyl chloride form by treatment with oxalyl chloride in a flask immersed in dry ice/acetone bath. The thus obtained 2-propylpentanoyl chloride was added to the amine solution dropwise followed by a dropwise addition of triethylamine (1 mL, 7.2 mmol). The reaction mixture was allowed to warm up to room temperature and was stirred overnight at 60°C. The solution was diluted with 25 mL of DCM, and washed with 5% HCL (2 × 100 mL) and with brine (100 mL). The organic layer was collected, dried over Na_2SO_4, and concentrated in vacuo. The product was purified using flash chromatography (column, 1" internal diameter, was packed with silica gel in hexanes, 6" to 8" height of the packed stationary phase). The purification (stationary phase: silica gel: eluent gradient: from 100% hexanes to 100% ethyl acetate) afforded 110 mg (0.25 mmol, 30% yield) of 5Pip. ^{1}H NMR (600 MHz, $CDCl_3$) δ/ppm: 10.45 (1 H, s), 8.36 (1 H, d, $J = 9.2$ Hz), 7.02 (2 H, m), 5.0 (1 H, $J = 9.2$ Hz), 4.09 (1 H, m), 3.04 (4 H, m), 2.22 (1 H, dt, $J = 9.2$, 4.6 Hz), 1.71 (4 H, dt, $J = 11$, 5.8 Hz), 1.63 (2 H, m), 1.53 (4 H, m), 1.34 (12 H, m), 0.9 (6 H, p, $J = 7.2$ Hz), 0.86 (6H, m). ^{13}C NMR (150 MHz, $CDCl_3$) δ/ppm: 174.70, 168.83, 147.45, 131.84, 123.04, 122.77, 120.72, 115.54, 51.91, 49.22, 49.00, 37.50, 35.40, 25.66, 23.82, 20.74, 19.20, 14.08, 13.97. HRMS (*m/z*, ESI-TOF): calcd. for $C_{27}H_{46}N_3O_2^+$, 444.3590 $[M + H]^+$; found, 444.3692.

Methods.—CV measurements were conducted using Reference 600 Potentiostat/Galvanostat/ZRA (Gamry Instruments, PA, U.S.A.), connected to a three-electrode cell equipped with a glassy carbon working electrode, an SCE reference electrode (connected to the cell via a salt bridge), and a platinum counter electrode, as previously described.[32,33] The salt bridge was filled with a saturated KCl solution. Anhydrous acetonitrile (MeCN) was employed with different concentrations of a supporting electrolyte, $N(C_4H_9)_4PF_6$, $N(C_4H_9)_4BF_4$ and $LiClO_4$. Prior to recording each voltammogram the sample is extensively purged with argon while maintaining its volume constant by adding more of the anhydrous solvent. For each sample, a set of voltammograms is recorded where the electrolyte concentration is increased from 25 mM to 200 mM in increments of 25 mM, at scan rates, $v = 10$, 20, 50, 100, 200 and 500 mV s^{-1}. For each sample and at each of the conditions and the scan settings, a triplicate of triplicates was measured, and the reported error bars represent plus-minus one standard deviation. That is, the same sample was measured three times in three different days, and at each measurement three voltammograms were recorded.

Analysis of the voltammograms and the obtained electrochemical potentials was carried out using Igor Pro, v. 7.02 (WaveMetrics, Inc., Lake Oswego, Oregon, U.S.A.). The half-wave potentials, $E^{(1/2)}$, are determined from the midpoints between the cathodic and anodic peak potentials, E_a and E_c, respectively. E_a and E_c are determined from the zero points of the first derivatives of the voltammograms, i.e., the potentials where $\partial i/\partial E = 0$ at $\partial E/\partial t =$ constant. The inflection point potentials, $E^{(i)}$, are determined from the zero points of the second derivatives at the rising spans of the anodic waves of the voltammograms, i.e., the potentials where $\partial^2 i/\partial E^2 = 0$ at $\partial E/\partial t =$ constant. When the signal-to-noise ratios of the second derivatives are not high enough, they are smoothed using 4th order Savitzky-Golay algorithm. Linear fits of the voltammogram sections after the initial capacitance rise and before the faradaic wave provide the estimates for the baselines. Similar linear fits of the anodic waves after the beginning of the initial faradaic rise and before the curvature leading to the peak yields the anodic asymptotic lines. The edge potentials, $E^{(e)}$, are estimates from the points where these asymptotes cross the baselines. The peak heights, p, is determined from the current difference between the anodic peak and inclined baseline at the peak potential. The potentials at the points on the rising anodic wave that corresponds to p/2 provide the estimates for $E^{(p/2)}$. Functions, built in Igor Pro, were used for the statistical tests that produced the p-values.

General Considerations

For reversible processes, the CV-obtained values of $E^{(1/2)}$ offer excellent estimates for $E^{(0)}$. Irreversibility or partial reversibility, however, are significantly more prevalent than reversibility, especially for organic and bioorganic redox couples, and for protic and other potentially reactive media. Oxidative or reductive degradation, dimerization, reactions with the solvent, relatively fast mass transport and other processes that deplete the electrochemically produced species at the surface of the working electrode, strongly affect the recorded cyclic voltammograms making them "asymmetric" and even completely eliminating the anodic or the cathodic peak.

The pressing question at hand is how well $E^{(i)}$, $E^{(p/2)}$, $E^{(p)}$, and $E^{(e)}$ can serve as estimates for $E^{(0)}$ when $E^{(1/2)}$ is not available? The shapes of the voltammogramic waves depend on the electron-transfer kinetics, mass transport dynamics and scan rates, as well as on chemical reactions that deplete the analyte from the surface of the working electrode. For example, an increase in the scan rate can improve the reversibility if the lifetimes of the electrocehcmially produces species are comparable with the time spans between the beginning of the forward-scan wave and the end of the back-scan one. An increase in the scan rates, however, pushes the peak potentials away from $E^{(1/2)}$. Therefore, if reversibility is not achieved, increasing the scan rates can prove detrimental, especially when $E^{(p)}$ provides the metrics for $E^{(0)}$. Concurrently, reversing the direction of the scans at potentials as soon as possible after the peak of the forward-scan waves can also improve the reversibility of the cyclic voltammograms. Bringing the

potential of the scan reversal too close to the peak, however, can alter its shape and shift $E^{(p)}$.

The values of $E^{(p)}$ are most frequently reported for potentials of processes displaying irreversible voltammograms. The positons of the peaks of the voltammogramic waves, however, strongly depend on the scan rates, the sample concertation, and the kinetics of interfacial electron transfer especially when side reactions deplete the analyte from the electrode surface. Hence, $E^{(p)}$ is not invariant to the experimental settings. Inherently, the peak potentials can never overlap with $E^{(1/2)}$, and with $E^{(0)}$. Therefore, two-dimensional extrapolation of $E^{(p)}$ to zero scan rate and zero sample concentrations from multiple measurements is the way to obtain values from the peak potentials that are close to $E^{(0)}$.

Conversely, $E^{(e)}$ represents the potential at which the Fermi level of the working electrode approaches the energy level of the frontier orbital of the analyte and the interfacial electron transfer becomes detectable. The edge potentials, therefore, are inherently sensitive to temperature. An increase in the temperature of the electrode conductive material broadens the energy distribution of the electrons above and the holes below the Fermi energy level. Despite it, the values of $E^{(e)}$ are inherently invariant to most other experimental settings. Nevertheless, $E^{(e)}$ cannot overlap with, and even approach, $E^{(1/2)}$. Furthermore, from a practical point of view, the capacitance and the ohmic currents affect the baseline of the voltammograms needed for estimating $E^{(e)}$.

Overall, $E^{(p)}$ overestimates reduction potentials of oxidation and $E^{(e)}$ underestimates them. Conversely, the values of $E^{(i)}$ and $E^{(p/2)}$ are always between those of $E^{(e)}$ and $E^{(p)}$. It is reasonable to hypothesize, therefore, that $E^{(i)}$ and $E^{(p/2)}$ offer the best readily accessible estimates for $E^{(0)}$ when $E^{(1/2)}$ is not attainable.

The standard electrode potential, $E^{(0)}$, is a fundamental thermodynamic characteristic of a redox couple and as such, its estimated values should be invariant to the experimental settings. In condense phase, indeed, the media affects the electronic properties of analytes. The heterogeneous nature of electrochemical processes presents further challenges. How do the electrode material and the composition of the electrolyte solution near the electrode surface affect the solvation energy of the charged components of a redox couple? While extrapolation to zero salt concentration can eliminate the effects of the supporting electrolytes and produce the potentials of the redox couples for neat solvents,[32] it does not compensate for potential "artifacts" that may originate from certain types of working electrodes.

The material of the working and the counter electrodes should be inert. Thus, gold and platinum present good choices for such electrodes, except when the samples contain sulfur at low oxidation states. Thiols and other sulfur compounds have an immense affinity for coinage metals and may affect the recorded voltammograms. Concurrently, gold is a soft metal and routine mechanical chelating may compromise the smoothness of its surface. These challenges with noble metals, in addition to their cost, have made glassy carbon a preferred material for working electrodes for electrochemical analysis.

The morphology of the electrode surface also affects the recorded voltammograms, especially when sharp edges and roughness are essential for the nucleation of a new phase. For example, the overpotential for water reduction on mercury is huge because hydrogen bubbles cannot nucleate easily on its atomically flat surface. Therefore, mercury cathodes can readily reduce Na^+ to metal sodium from aqueous solutions to form liquid Na/Hg amalgam. The high solubility of sodium metal in mercury also helps for driving this process. In addition, mercury always exposes new pristine surface when forming a drop. While the Hg susceptibility to oxidation reduces its anodic window, dropping mercury electrode has been an indispensable choice for analyzing reduction processes. Its toxicity, however, has diminished the enthusiasm for its use. The morphology of electrode surface can control the selectivity of one process over another. Attaching a catalyst to the surface of an electrode offers the best way for attaining specificity of an interfacial process and observe thermodynamic limits of of a redox reaction.

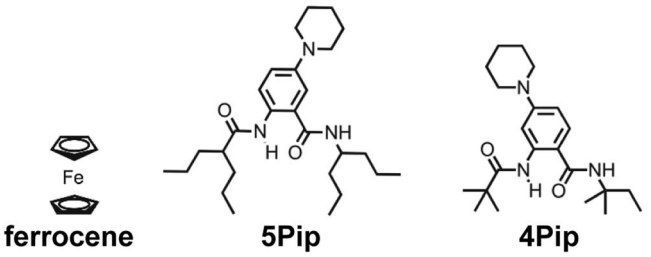

Chart 1. Analytes used for this study.

The dynamics of mass transport to and from the electrode surface also affects the recorded voltammograms. Agitating the solvent (e.g., purging with inert gas during data acquisition) and moving the electrode (e.g., using a rotating disc electrode) improve the efficiency of bringing fresh analyte to the electrode surface. It also aids the removal of the electrochemically generated species from the electrode surface and compromise the reversed waves. Therefore, rotating disc electrodes are invaluable for mechanistic studies of the dynamics of interfacial processes employing linear voltammetry, rather than CV. Similarly, using small electrodes (e.g., with area smaller than about 100 μm^2) enhances the edge effects, where the mass transport has multiple directions. Decreasing the working surface of an electrode increases the average mass-transport rates per unit area. Employing working electrodes with such small dimensions at relatively low scan rates, e.g., < 1 V s^{-1}, leads to cyclic voltammograms where the anodic and cathodic waves practically overlap and do not show apparent anodic and cathodic peaks, making it challenging to estimate $E^{(p)}$ and $E^{(1/2)}$. For a working electrode, therefore, we use a glassy carbon electrode with area of 7 mm^2.

Conducting CV measurements is relatively easy, which makes this technique as popular as it is. Setting up the reference electrode, however, can be a potential source for errors. While, for example, pseudoreference electrodes, such as silver wires, have their role in broadening the field,[34–46] they inherently have a range of shortcomings that are beyond the scope of this discussion. Conversely, we employ saturated calomel electrode (SCE) that, when not in use, we store in saturated aqueous solution of KCl. To prevent cross-contamination with the sample, we use a salt bridge for connecting the SCE electrode with the cell. Ideally, the salt bridge should contain the same solution with which the reference electrode is filled. It ensures that the electrolyte composition inside the electrode remains unchanged, and hence, prevents drifts of its potential during extended use.

When the reference electrode is water-based, however, such aqueous salt bridges present two practical issues for organic electrochemical analysis: (1) huge junction potentials between the bridge and the electrolyte solutions of the cell when using low-polarity solvents, such as $CHCl_3$ and CH_2Cl_2; and (2) water leakage from the bridge into the cell, which may present challenges when the dryness of the organic solution is important for the analysis. The use of a salt bridge that contains electrolyte solution in a moderately polar water-miscible organic solvent, such as acetonitrile and DMF, present a means for addressing both of those issues. Such a setup splits the huge junction potential into two moderate ones: at the bridge-electrode and the bridge-cell interfaces. Also, leaking an aprotic organic solvent with a wide electrochemical window into the sample solution is a better alternative to leaking water. This setup, however, is not ideal, either. Although it is slow, the diffusion of the component of the organic solution in such bridges across the frit of the reference electrode can cause drifts in the potential during extended use. Therefore, regular monitoring of the performance of the reference electrode, using samples with well-known potentials, is paramount for electrochemical analysis.

For analysis of reversible oxidation, we focus on ferrocene (Chart 1), which is one of the most broadly studied compounds in analytical electrochemistry and its voltammograms manifest pronounced reversibility.[47–50] In voltammetry, therefore, ferrocene has gained popularity as a convenient internal standard and frequently potentials are

reported vs. its oxidation.[51–53] As robust as the ferrocene-ferrocenium redox couple is, its use for a reference should be approached with caution. The reduction potential of ferrocenium strongly depends on the solvent polarity and the electrolyte concentration.[32] (According to the accepted convention, $E^{(0)}$ represents the reduction potentials of the oxidized components of redox couples, regardless whether the voltammograms examine the reduction or oxidation propensity of the analyte).[54,55]

To illustrate CV analysis of irreversible and partially reversible oxidation, we focus on electron rich anthranilamide residues that we developed as building blocks for hole-transfer bioinspired molecular electrets.[56–60] Placing an amine on position 5, such as in 5Pip (Chart 1), stabilizes the radical cation and leads to reversible electrochemical behavior.[22,25] Moving the amine to position 4, however, e.g., 4Pip (Chart 1), causes a positive shift of the anodic wave along with irreversible behavior.[22,25] We demonstrated that eliminating the proton on the C-terminal amide of 4Pip and replacing it with an alkyl group stabilizes the radical cation, $4Pip^{\bullet+}$, leading to voltammograms showing partial reversibility and showing that the amide proton is involved in the oxidative degradation of 4Pip.[22] In this study, we test if the α-protons on the aliphatic chains attached to the two amides are responsible for the decomposition of $4Pip^{\bullet+}$. Therefore, we use a derivative of 4Pip capped with tertiary alkyl substituents (Chart 1).

For a solvent, we employ dry acetonitrile (MeCN) because its moderately high polarity minimizes the dependence of the measured potentials on the electrolyte concentration, C_{el}.[32,33] Nevertheless, we still extrapolate the measured potentials to $C_{el} = 0$ (Figure 2), estimating their values for the neat solvent.[32,33] The extrapolated values of $E^{(1/2)}$ for electrolyte-free media relate the electrochemical findings with results from optical studies,[26,32,61] which prove especially invaluable for analyzing systems mediating photoinduced charge transfer.[23,31,62]

The best way to validate the extrapolation of potential values to $C_{el} = 0$ is to test the same analyte with different electrolytes in the same solvent. Furthermore, the extrapolated potentials should be invariant to the sample concentration. For three different supporting electrolytes and ferrocene concentration between 1 and 20 mM, the extrapolation to $C_{el} = 0$ yields values for $E^{(1/2)}$ that are the same within experimental uncertainty (Figure 2). This finding validates the extrapolation approach for estimating $E^{(1/2)}$ for neat solvents.

Conversely, the trends of $E^{(1/2)}$ vs. C_{el} reveal two features that are important for CV experimental designs. First, an increase in ferrocene concentration increases the standard deviations of the extrapolated potentials (Figure 2b). That is, increasing the analyte concentration increases the uncertainty of estimating the potentials for neat solvents, which appears to originate from deviations of the $E^{(1/2)}$ values for small C_{el}. This finding strongly suggests that the concentration of the supporting electrolyte should exceed the concentration of the analyte by at least a factor of 5 or 10.

Second, while lowering the electrolyte concentration converges $E^{(1/2)}$ to the same value, there is a significant difference between the potentials for perchlorate and the other two electrolytes (Figure 2a). Also, the values of $E^{(1/2)}$ for $LiClO_4$ show stronger dependence on C_{el} than those for the PF_6 and BF_4 salts. While increasing the concentration of the supporting electrolyte improves the conductance of electrochemical cells and decreases the ohmic current (i_O), it also changes the dielectric constant of the solvent (ε). About ten years ago, we demonstrated that this variation in the dielectric properties of the media is responsible for the dependence of $E^{(1/2)}$ on C_{el} for electrolytes with bulky polarizable ions, such as $N(C_4H_9)_4PF_6$ and $N(C_4H_9)_4BF_4$.[32] The results for $LiClO_4$ appear to suggest that this salt drastically changes the properties of acetonitrile. Indeed, as a hard Lewis acid, Li^+ can affect the structure of solvents such as acetonitrile.[63] Still, it is unlikely for the lithium ions of the electrolyte to increase the dielectric constant of the solution to a large enough extent to induce 100-mV negative shifts of $E^{(1/2)}$ (Figure 2a). Considering the Born solvation energy, $E^{(1/2)}$ is proportional to $(1 - \varepsilon^{-1})$.[32,64] For polar media, therefore, variations in ε will have quite smaller effect on ε^{-1} (and on the reduction potentials) than for non-polar solvents.[32,33] Hence, differences in the interactions between the electrolyte ions and the solvent cannot singlehandedly provide an explanation for the observed trends (Figure 2a).

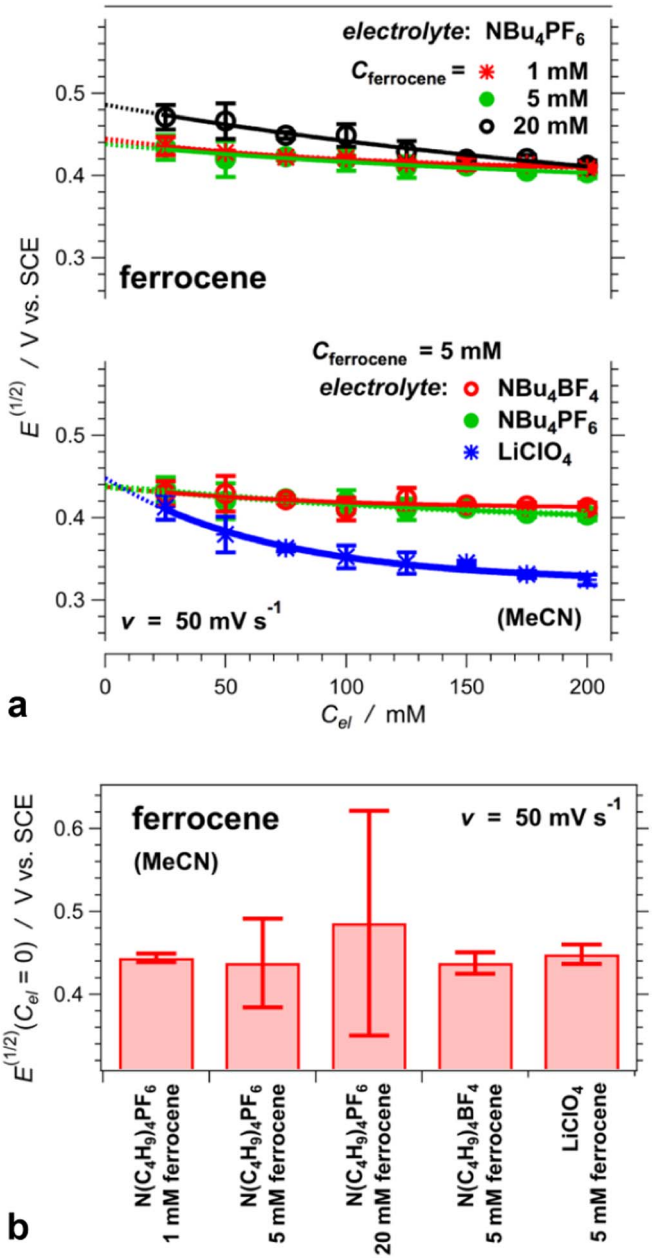

Figure 2. Extrapolation of the half-wave potentials of ferrocene to zero electrolyte concentration using different electrolytes and different ferrocene concentrations recorded at 50 mV s^{-1}. (a) Dependence of the half-wave potentials on the electrolyte concentration. The solid lines represent the data fits and the dotted lines – extrapolation to zero. (b) Comparison between the half-wave potentials obtained from the extrapolation to zero electrolyte concentration.

Recently, Miller et al. demonstrated the drastic effects that pairing with the ions of the supporting electrolyte can have on electrochemical potentials.[65] The anions of the three electrolytes, PF_6^-, BF_4^- and ClO_4^-, have similar radii and comparable electronic properties.[66] Conversely, $N(C_4H_9)_4^+$ and Li^+ are distinctly different. Unlike $N(C_4H_9)_4^+$, small alkaline ions, such as Li^+ and Na^+, have a strong propensity for coordination with oxygen-containing ligands, such as water. In organic solvents, which cannot provide such ligation, these cations are often prone to aggregation with the analyte. As an electron-rich compound, ferrocene has nucleophilic properties[67–69] and a propensity for binding alkaline ions,[70] especially Li^+.[71–73]

Binding lithium ions adds positive charges to the complexes with ferrocene and should impede the extraction of electrons. Hence, $LiClO_4$ should cause a positive shift in the reduction potential, which is contrary to what we observe (Figure 2a).

While electrochemical potentials correlate with the energy levels of the frontier orbitals of the analyte,[74–81] $FE^{(0)}$ and $FE^{(1/2)}$ of the oxidation and reduction do not measure the energies, respectively, of the highest occupied molecular orbitals (HOMOs) and the lowest unoccupied molecular orbitals (LUMOs). That is, the negative $E^{(1/2)}$ shifts, induced by $LiClO_4$ (Figure 2a), do not indicate that the electrolyte raises the HOMO energy of ferrocene. Rather, $FE^{(1/2)}$ measures energy differences between the oxidized and the reduced forms of the analyte. Differences between the solvation energies of these two forms further modulate $E^{(1/2)}$. The change in the analyte charge during oxidation or reduction is the principal contribution to these solvation-energy differences.

Therefore, a loss of a lithium ion during the oxidation of Li^+-ferrocene complexes can account for the observed trends (Figure 2a). In addition to an entropic gain, oxidizing a Li^+-ferrocene complex to a ferrocenium ion conserves the positive charge on the analyte and minimizes the changes in the solvation energy, assuming that the excess number of ClO_4^- counterions can readily "assimilate" the released Li^+ ions. In this manner, Li^+ interaction with ferrocene can improve the ease of its oxidation and lower the reduction potential (Figure 2a).

Overall, the supporting electrolyte is not necessarily a passive component of the samples. For the rest of the study, we employ $N(C_4H_9)_4PF_6$, and limit the analyte concentration to 1 mM to ensure reliable extrapolation to $C_{el} = 0$.

Results and Discussion

Reversible oxidation.—The first and the second derivatives of cyclic voltammograms are immensely instrumental for determining some of the key potentials of the analyte (Figures 3a,3b). The zero values of the first derivatives, $\partial i/\partial E = 0$, yield the peak potentials, E_a and E_c, essential for calculating $E^{(1/2)}$, i.e., $E^{(1/2)} = (E_a + E_c) / 2$ (Figure 3b). Also, for oxidation, the peak potentials of interest correspond to the anodic peaks, i.e., $E^{(p)} = E_a$. The potentials at which the second derivatives assume zero, $\partial^2 i/\partial E^2 = 0$, represent the inflection points of the voltammograms and provide a straightforward way for determining $E^{(i)}$ (Figure 3b).

The derivatives also reveal a range of subtle details that are not truly apparent in the voltammogram. After all, differentiation eliminates the offset induced by i_C and yields in a constant value for the small linear rise due to i_R (Figures 1, 3). Visual inspection of the derivatives allows for facile examination of the reversibility. If a process is reversible, the first derivatives of its cyclic voltammograms have axial symmetry across $E = E^{(1/2)}$ with the forward and back sweep crossing at $E^{(1/2)}$ (Figure 3c). In addition, reversibility yields second derivatives that are centrosymmetric around the point on the ordinate corresponding to the half-wave potential, i.e., ($E^{(1/2)}$,0) (Figure 3d). As revealed by their derivatives, all voltammograms of ferrocene manifest reversibility.

The cyclic voltammograms of irreversible oxidation does not show cathodic peaks and cannot provide a means for estimating $E^{(1/2)}$ from E_a and E_c. Therefore, using the characteristic of the anodic waves of reversibly oxidizable ferrocene provides the ideal means for examining which of the potentials have values close to those of $E^{(1/2)}$. In addition to $E^{(i)}$ and $E^{(p)}$, which we estimate from the derivatives of the voltammograms, we also examined $E^{(p/2)}$ and $E^{(e)}$. The half-height peak potential, $E^{(p/2)}$, corresponds to the potential of the rising anodic wave that is in the middle between the peak and the baseline (Figures 1, 3b). The crossing of the asymptotic lines of the baseline and the rising anodic wave provides the estimates for the edge potentials $E^{(e)}$ (Figures 1, 3b).

Because $E^{(0)}$ is a fundamental characteristic, it is invariant to experimental parameters, such as scan rate (v). To examine the invariance of the different potentials on the scan rates (Figure 4), we resort to a linear regression analysis with a null hypothesis (H_0) that the linear relationship E vs. v has a slope 0. The calculated p-values represent the probability to obtain the measured potentials if H_0 is correct. While such analysis does not validate H_0, it can readily allow rejecting H_0 when p is a small number, i.e., when $p < \alpha$, and $\alpha = 0.01$, 0.05 or 0.1 depending on the selected confidence interval. The immensely small p-values for $E^{(p)}$, $E^{(i)}$ and $E^{(p/2)}$, extracted from voltammograms of samples with different electrolyte concentrations (Table I), clearly show that we can readily reject the H_0 for these potentials. We can also reject H_0 for $E^{(e)}$ for $\alpha = 0.05$ or larger. That is, $E^{(p)}$, $E^{(i)}$, $E^{(e)}$ and $E^{(p/2)}$ show dependence on v with 95% confidence (Figure 4a). Examining the scan-rate dependence of the extrapolated potentials for neat solvent reveal the same trends (Figure 4b). While the extrapolation increases the uncertainty and the p-values, we can still reject the H_0 for $E^{(p)}$, $E^{(i)}$ and $E^{(p/2)}$ with the same confidence of 95% (Table I).

The edge potential, $E^{(e)}$, appears to show some invariance to v (Figure 4). Despite the relatively small uncertainty (small standard deviations) of its estimates, its p-values are not too small, i.e., $p > 0.01$ for $C_{el} = 100$ mM and $p > 0.1$ for a neat solvent. This finding indicates that the inception of the faradaic signal does not have a strong dependence on the scan rate, which is consistent with large electron-transfer rates and with a relatively large amount of analyte adsorbed on the surface of the working electrode.

Because of the lack of invariance with v for most of the potentials, we test how close $E^{(p)}$, $E^{(i)}$, $E^{(p/2)}$ and $E^{(e)}$ are to $E^{(1/2)}$ for each scan rates. We employ a Welch's analysis of variance (ANOVA) where H_0 states that the means of the compared potentials are the same, and the p-values represent the probability of obtaining the observed values when H_0 is correct. While small p-values, i.e., $p < \alpha$, permit rejection of H_0, ANOVA does not provide the basis for accepting H_0 when $p > \alpha$.

For data directly obtained from the measured voltammograms, e.g., for $C_{el} = 100$ mM, we can clearly reject H_0 for $E^{(e)}$ and $E^{(p)}$ with 95% confidence (Table II). That is, the peak potentials and the edge potentials are not a good representation of $E^{(1/2)}$, and of $E^{(0)}$ for that matter. For $E^{(p/2)}$, only $v = 200$ and 500 mV s^{-1} yield p larger than about 0.05 and we can reject H_0 with 95% confidence for most of the examined scan rates (Table II). Hence, $E^{(p/2)}$ is not a good representation of $E^{(1/2)}$ and of $E^{(0)}$ for small scan rates.

The ANOVA tests for the inflection potential, $E^{(i)}$, appear most encouraging. If we adopt a less conservative 90% confidence, we can perhaps reject H_0 only for 10 and 20 mV s^{-1}. With 95% confidence, however, we cannot truly reject H_0 for any of the scan rates for $E^{(i)}$. While ANOVA does not validate the acceptance of H_0, these findings imply that the inflection potentials provide the best estimates for $E^{(0)}$, when $E^{(1/2)}$ cannot be calculated due to irreversibility, for example.

The extrapolation of the different potentials to $C_{el} = 0$ adds uncertainty in their estimates, which affects the outcome of the ANOVA tests. While the trends appear the same, the p-values for the extrapolated potentials are larger than the p-values for those obtained directly from the voltammograms, e.g., for $C_{el} = 100$ mM (Table II). With 95% confidence we can still reject H_0 for the edge potentials even at $C_{el} = 0$, confirming that $E^{(e)}$ does not provide a good estimate for $E^{(0)}$. We cannot reject H_0 for any of the other cases for $C_{el} = 0$, except perhaps for $E^{(p)}$ at 500 mV s^{-1}, assuming 90% confidence (Table II).

Overall for oxidation of ferrocene, the inflection potentials, $E^{(i)}$, provides the best estimates for $E^{(0)}$ (Table II). The half-peak potentials, $E^{(p/2)}$, also appear promising for representing $E^{(0)}$, especially for larger scan rates. The peak potentials, $E^{(p)}$, are positively shifted from $E^{(1/2)}$ by 30 to 100 mV (Figure 4). With this level of uncertainty, however, the peak potentials, $E^{(p)}$, could be representative of $E^{(1/2)}$ but only for small scan rates. In contrast, for all cases the edge potentials, $E^{(e)}$, underestimate $E^{(1/2)}$ by about 70–80 mV for all scan rates (Figure 4), and should not be used for representing $E^{(0)}$.

While $E^{(1/2)}$ and $E^{(e)}$ are invariant to v, an increase in the scan rate causes positive shifts of $E^{(p)}$, $E^{(p/2)}$ and $E^{(i)}$ (Figure 4). These shifts bring the values of $E^{(p)}$ away from $E^{(1/2)}$ and the values of $E^{(i)}$ and $E^{(p/2)}$ closer to $E^{(1/2)}$. While at truly small scan rates, peak potentials can represent $E^{(0)}$ with some uncertainty, the values of $E^{(p)}$ can never overlap with those of $E^{(1/2)}$. Conversely, an increase in the scan rates

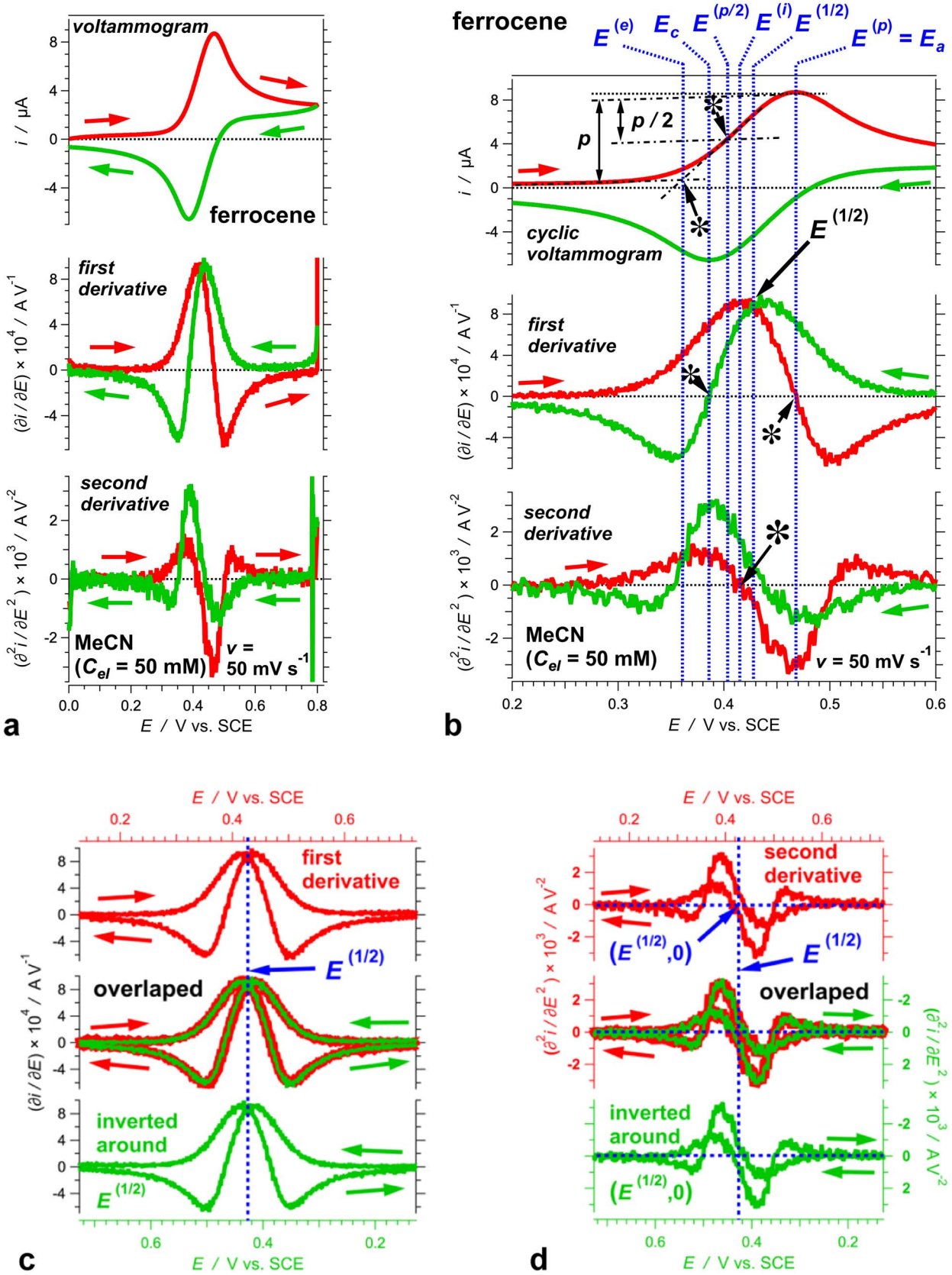

Figure 3. Cyclic voltammogram and its derivatives of ferrocene (1 mM), recorded in the presence of 50 mM $N(C_4H_9)_4PF_6$ as a supporting electrolyte at 50 mV s^{-1}. (a) The voltammograms and its first and second derivatives where different colors represent the forward and the back scans as designated by the arrows. (b) Representation of the voltammogram and its derivatives, zoomed on the anodic and the cathodic waves, with designation of the different potentials of interest. (c) Demonstration of the axial symmetry of the first derivative. The derivative (upper curve) and its representation inverted around $E = E^{(1/2)}$ (lower curve) overlap perfectly (middle curves). (d) Demonstration of the centrosymmetric shape the second derivative. The derivative (upper curve) and its representation inverted around $E = E^{(1/2)}$ and around $i = 0$ (lower curve) overlap perfectly (middle curves).

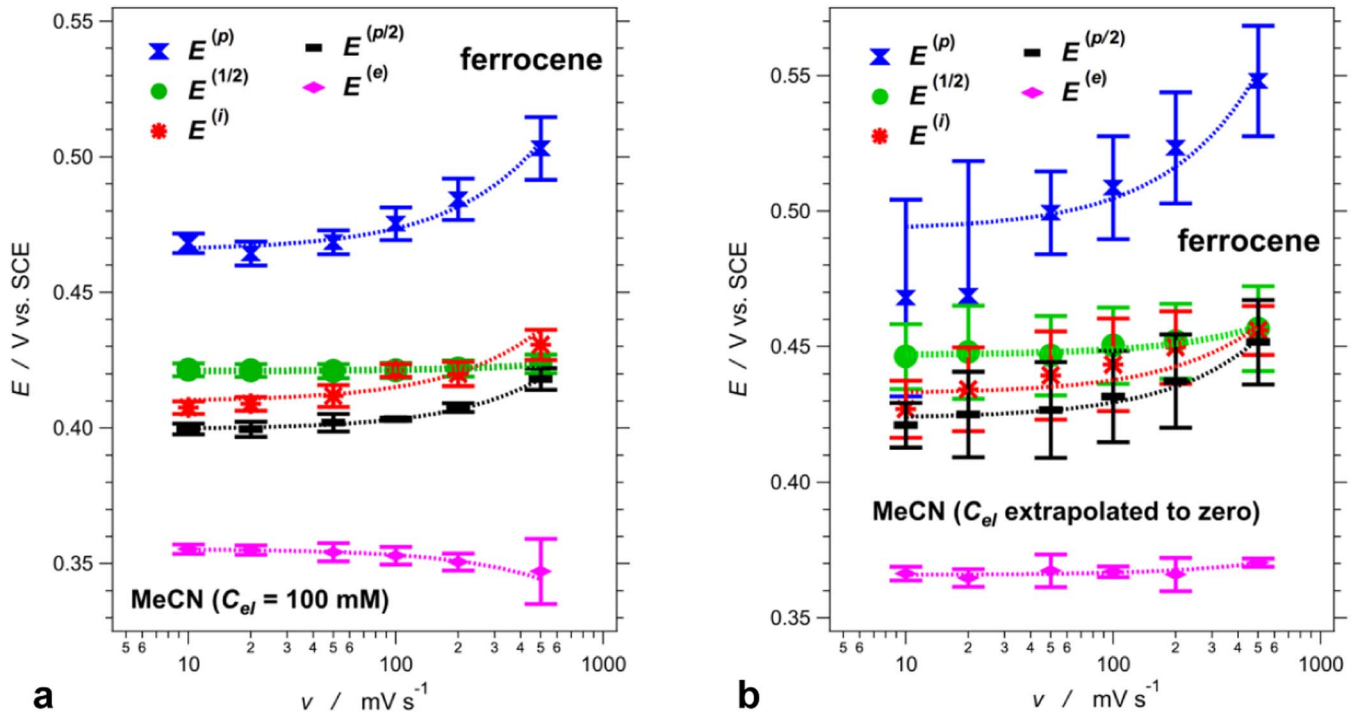

Figure 4. Dependence of the different potentials of ferrocene (1 mM) on the scan rate. (a) The potentials are obtained from voltammograms recorded for samples containing 100 mM $N(C_4H_9)_4PF_6$ as a supporting electrolyte. (b) The potentials are obtained from extrapolation to zero electrolyte concentration.

makes $E^{(i)}$ closely overlap with $E^{(1/2)}$ for v of 100 mV s^{-1} and larger (Figure 4). The values of $E^{(p/2)}$ show a similar trend and an overlap with $E^{(1/2)}$ at 500 mV s^{-1}. For the examined scan rates, however, the half-peak potentials show larger underestimates of $E^{(1/2)}$ than $E^{(i)}$, making the inflection potentials the preferred representation of $E^{(0)}$ when $E^{(1/2)}$ is inaccessible.

When partial irreversibility is not obvious.—Ferrocene-ferrocenium is an extensively studied well-behave redox couple and serves as an excellent model for testing concepts and ideas. To further validate and expand the findings from the ferrocene studies, we focus on an electron-rich amidated non-native amino acid, 5Pip (Chart 1), the dipole of which can induce significant rectification of charge transfer.[31]

The cyclic voltammograms of 5Pip show excellent reversibility in anhydrous media, especially for polarizable solvents, such as CH_2Cl_2.[22,25] We observe similar behavior of 5Pip for this setup with aqueous salt bridge, but only at high scan rates (Figures 5a, 5b). At scan rates of 10 and 20 mV s^{-1}, however, the cathodic wave appears smaller than the anodic peak; and an additional small cathodic peak at about 0.3 V vs. SCE becomes apparent (insets of Figures 5a, 5b).

Table I. *p*-values from linear regression tests of the dependence of the different potentials on the scan rate.[a]

potential	C_{el} =	ferrocene 100 mM	ferrocene 0 mM [b]	5Pip 0 mM [b]
$E^{(1/2)}$		0.14	0.27	0.054
$E^{(i)}$		5.1×10^{-6}	0.014	4.2×10^{-4}
$E^{(p/2)}$		2.5×10^{-9}	6.8×10^{-3}	5.6×10^{-4}
$E^{(p)}$		1.7×10^{-7}	3.3×10^{-3}	3.7×10^{-5}
$E^{(e)}$		0.023	0.11	0.20

[a]H_0: The relation E vs. v has a slope 0. Small p-values permit rejection of H_0 and suggest that E depends on v.
[b]From extrapolation to zero electrolyte concentration.

The first derivatives of the cyclic voltammograms of 5Pip clearly show a lack of symmetry for small scan rates, which is consistent with deviation from reversibility (Figure 6). As the scan rates increase, the first derivatives gradually gain symmetry and the additional cathodic peak at 0.3 V vs. SCE becomes less apparent. At 500 mV s^{-1}, the oxidation is practically reversible, i.e., the first derivative exhibits axial symmetry across $E^{(1/2)}$, and the area of the second cathodic peak drops to less than 5% of the area under the anodic wave.

These findings are consistent with degradation of the oxidized analyte, $5Pip^{\bullet+}$, within the timescales of acquisition at small scan rates. The timespans between the beginning of the anodic and the completion of the cathodic waves range from about 2 s, for 500 mV s^{-1}, to about 70 s, for 10 mV s^{-1} (Figure 6c). Hence, the observed partial reversibility is consistent with a lifetime of $5Pip^{\bullet+}$ that is in the order of 100 s under the conditions of the measurements.

Regardless the partial irreversibility, the presence of anodic and cathodic peaks allows for estimating the half-wave potentials of 5Pip for different scan rates and electrolyte concentrations. Extrapolation to $C_{el} = 0$ yields similar values of $E^{(1/2)}$ for the different scan rates (Figure 5c). Increasing v from 10 to 500 mV s^{-1} increases $E^{(1/2)}(C_{el} = 0)$ from about 0.73 to 0.75 V vs. SCE (Figure 7). The results for $E^{(1/2)}$ at 500 mV s^{-1} are the best estimates for $E^{(0)}$ because of the reversibility at this scan rate. Despite the induced irreversibility, decreasing the scan rates by a factor of 50 changes $FE^{(1/2)}$ by less than k_BT. This finding has important implications, demonstrating that even for partially reversible behavior, $E^{(1/2)}$ still provides the best estimates for $E^{(0)}$.

The extrapolated potentials for a neat solvents show that $E^{(1/2)}$, $E^{(i)}$ and $E^{(p/2)}$ of 5Pip practically overlap (Figure 7), and the ANOVA tests yield large p-values when comparing $E^{(1/2)}$ with $E^{(i)}$ and $E^{(p/2)}$ (Table II). The values of $E^{(p)}$ and $E^{(e)}$ are distinctly separated from $E^{(1/2)}$ (Figure 7), and except for 10 mV s^{-1}, all p-values from the ANOVA test comparing $E^{(e)}$ with $E^{(1/2)}$ are smaller than 0.05 (Table II). While the differences between $E^{(p)}$ with $E^{(1/2)}$ are similar to those between $E^{(e)}$ with $E^{(1/2)}$, the ANOVA p-values for $E^{(p)}$ vs. $E^{(1/2)}$ are quite large due to uncertainty of estimating the peak potentials, which

Table II. *p*-values from Welch's ANOVA tests comparing $E^{(1/2)}$ with the other potentials.[a]

sample	C_{el} / mM	v / mV s^{-1}	($E^{(1/2)}$, $E^{(i)}$)	($E^{(1/2)}$, $E^{(p/2)}$)	($E^{(1/2)}$, $E^{(p)}$)	($E^{(1/2)}$, $E^{(e)}$)
ferrocene	100	10	0.050	0.019	8.2×10^{-3}	1.8×10^{-3}
		20	0.070	0.027	0.013	1.9×10^{-3}
		50	0.19	0.043	0.011	3.9×10^{-3}
		100	0.42	0.022	0.015	3.8×10^{-3}
		200	0.75	0.049	0.017	3.6×10^{-3}
		500	0.40	0.39	0.022	0.022
	0[b]	10	0.35	0.22	0.72	0.022
		20	0.61	0.43	0.73	0.041
		50	0.77	0.47	0.13	0.038
		100	0.78	0.48	0.13	0.028
		200	0.91	0.57	0.10	0.029
		500	0.97	0.84	0.071	0.032
5Pip	0[b]	10	0.68	0.31	0.23	0.067
		20	0.91	0.33	0.081	0.031
		50	0.65	0.47	0.10	0.027
		100	0.96	0.63	0.11	0.034
		200	0.94	0.99	0.076	0.021
		500	0.42	0.83	0.14	0.013

[a]H_0: $E^{(1/2)}$ and $E^{(x)}$ have the same means, where $x = i$, $p/2$, p and e. Small p-values permit rejection of H_0 and suggest that $E^{(1/2)}$ and $E^{(x)}$ have different values.
[b]From extrapolation to zero electrolyte concentration.

is similar to what we observe for ferrocene (Table II). While the statistical analysis does not allow the rejection of H_0, as an indication that $E^{(p)}$ vs. $E^{(1/2)}$ are significantly different, the large variations in the estimates $E^{(p)}$ (Figures 4b, 7) renders the peak potentials unattractive for quantification of molecular electronic characteristics.

Irreversible behavior.—For systems undergoing irreversible oxidation or reduction, $E^{(p)}$ (i.e., E_a or E_c, respectively) is the most frequent choice for representing their electrochemical potentials. This practice has a lot of shortcomings since the peak potentials are immensely sensitive to experimental settings (e.g., scan rate, sample concentration, and electrolyte concentration), and the inherent properties of the redox couples (e.g., rates of interfacial electron transfer and diffusion). The studies with ferrocene and 5Pip show that inflection and half-peak potentials provide good estimates of $E^{(0)}$, better than the peak potentials. To illustrate how they compare for irreversible oxidation, we choose another electron-rich non-native amino acid derivative, 4Pip (Chart 1), forming a radical cation that is unstable under the CV conditions.[22,25]

In anthranilamide (Aa) residues, moving the amine from 5th to 4th position (i.e., 5Pip vs. 4Pip) makes the oxidation of these derivatives completely irreversible due to a significant change in the spin-density distribution in their radical cations.[22] Extending the positive charge of Aa$^{\bullet+}$ moieties over their C-terminal amides leads to decomposition. A loss of an amide proton is a possible path for this oxidative degradation. As we showed, derivatizing 4Pip with a tertiary C-terminal amide, i.e., -C(O)N(R_2)-, induces partial reversibility.[22] It confirms that the C-terminal amide proton contributes to the instability of 4Pip$^{\bullet+}$ but is not solely responsible for the oxidative degradation.

Another possibility involves the alkyl α-protons next to the amides. In all Aa derivatives, these α-protons are deshielded, with chemical shifts downfield from those of the rest of the alkyl protons, which may make them labile enough under oxidative conditions. To test it, in this study we capped 4Pip amides with tertiary alkyl chains (Chart 1). For all scan rates and electrolyte concentrations, the cyclic

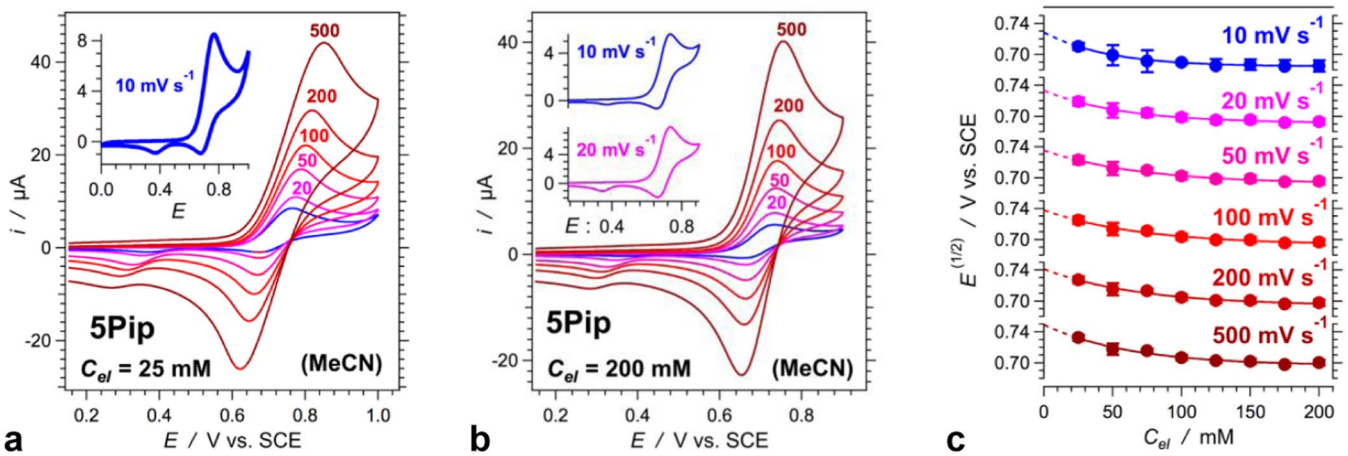

Figure 5. Cyclic voltammograms of 5Pip (1 mM) recorded at different scan rates in the presence of different concentrations of $N(C_4H_9)_4PF_6$ as a supporting electrolyte. (a,b) Voltammograms of samples containing 25 and 200 mM electrolyte. (c) Dependence of the half-wave potentials on the electrolyte concentration for the different scan rates. The solid lines represent the data fits and the dotted lines – the extrapolation to zero electrolyte concentration.

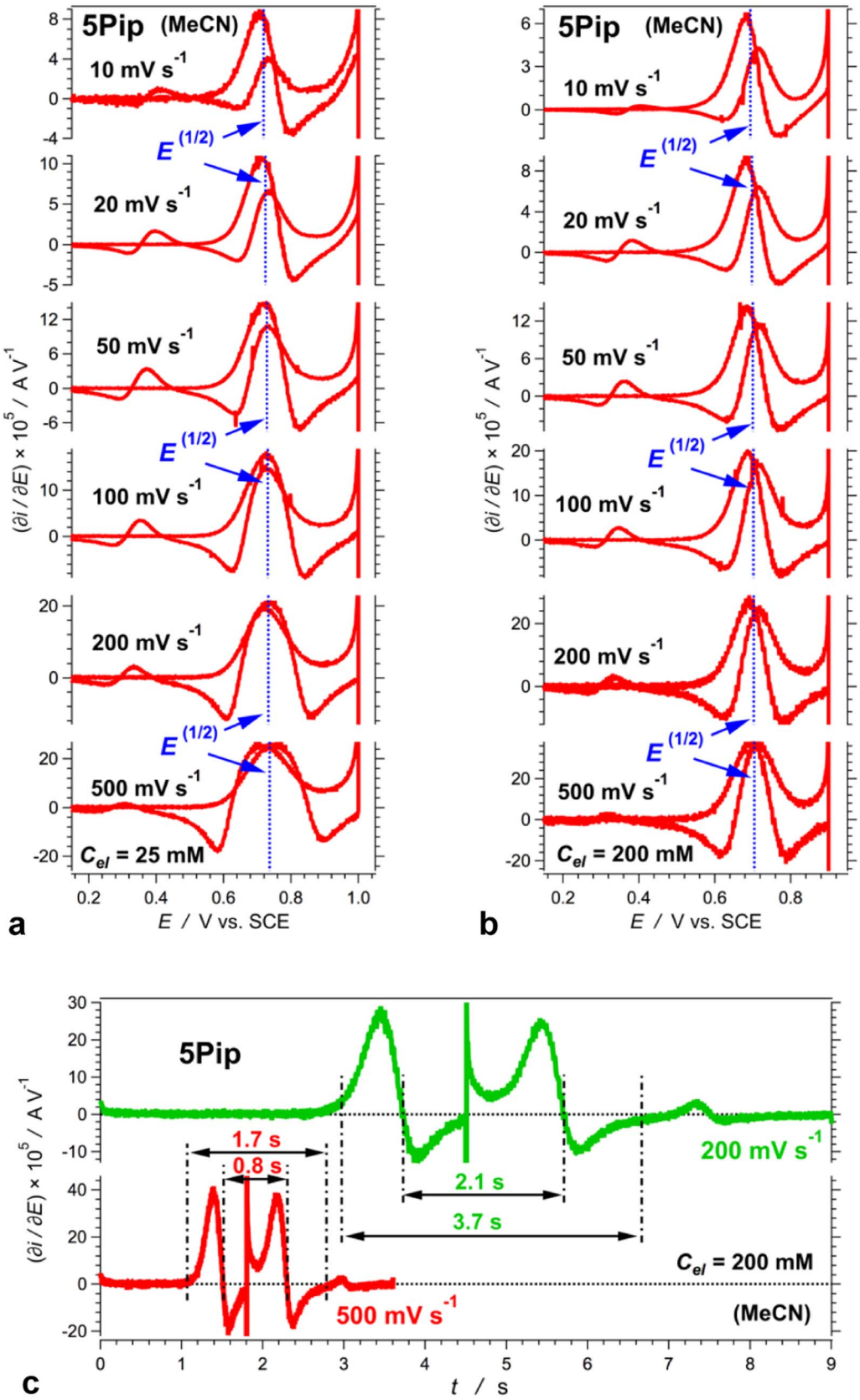

Figure 6. First derivatives of cyclic voltammograms of 5Pip (1 mM) recorded at different scan rates in the presence of 25 and 200 mM of $N(C_4H_9)_4PF_6$ as a supporting electrolyte. (a,b) the first derivatives. The obtained half-wave potentials are shown. (c) Dependence of the first derivatives on the scanning time showing the durations of data acquisition for different scan rates.

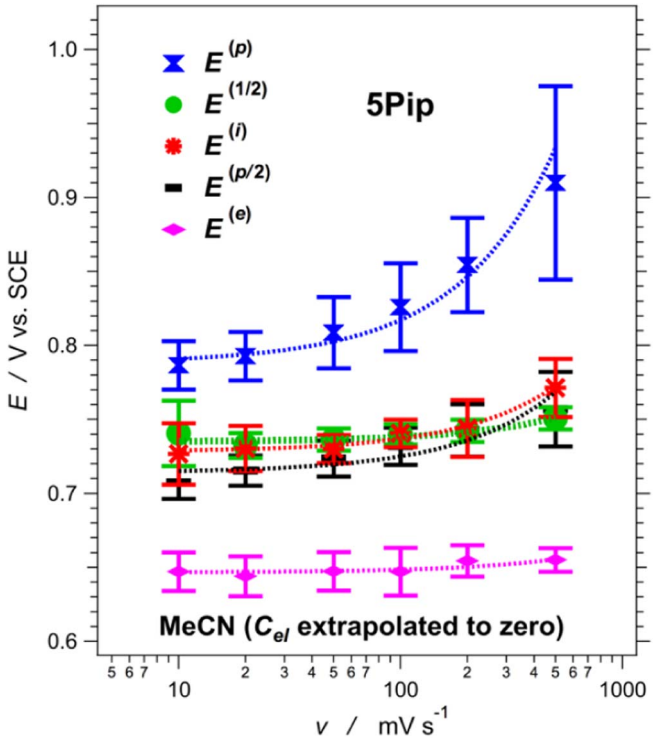

Figure 7. Dependence of the different potentials of 5Pip (1 mM) on the scan rate. The potentials are obtained from extrapolation to zero concentration of $N(C_4H_9)_4PF_6$ (Figure 5c).

voltammograms of the *t*-alkyl capped 4Pip show complete irreversibility, with no detectable cathodic peaks. Hence, removal of the α-protons next to the amides does not stabilize the radical cation of 4Pip for the timescales of the CV data acquisition.

The first and second derivatives of the cyclic voltammograms of the irreversible oxidation of 4Pip do not show symmetric features (Figure 8a). The derivatives of the anodic wave of 4Pip appear the same as those of ferrocene and 5Pip. It is, however, the derivatives of the cathodic waves that discern irreversible from reversible oxidation (Figures 3, 6, 8a).

Because the anodic waves of the voltammograms and their derivatives are quite similar for analytes undergoing reversible and irreversible oxidation, we can reliably use them for estimating $E^{(i)}$, $E^{(p/2)}$ and $E^{(e)}$, in addition to $E^{(p)}$ (Figure 8a), and extrapolate them to zero electrolyte concentration. Similar to 5Pip, the scan-rate dependence of the extrapolated potentials of 4Pip show clustering of the values for $E^{(i)}$ and $E^{(p/2)}$. Conversely, $E^{(e)}$ and $E^{(p)}$ are well separated from $E^{(i)}$ and $E^{(p/2)}$ (Figure 8b).

As the scan rates vary from 10 to 500 mV s^{-1}, $E^{(p)}$ of 4Pip increases with 150 mV, while $E^{(i)}$ and $E^{(p/2)}$ increase with about 80 mV (Figure 8b). For 4Pip, this increase in the potentials is predominantly at the small scan rates. Hence, between 100 and 500 mV s^{-1}, $E^{(i)}$ and $E^{(p/2)}$ of 4Pip vary within about 40 mV (i.e., less than $2k_BT$), while the $E^{(p)}$ of 4Pip varies over 100 mV (Figures 8b). Considering that reversible oxidation results in the best overlap of $E^{(1/2)}$ with $E^{(i)}$ and $E^{(p/2)}$ at scan rates between 100 and 500 mV s^{-1} (Figures 4, 7), which is the range where $E^{(i)}$ and $E^{(p/2)}$ of 4Pip show the smallest dependence on *v*, makes the inflection and half-peak potentials the best estimate for $E^{(0)}$ of the irreversibly behaving systems, 4Pip.

Pros and cons of inflection potentials.—Our studies reveal that inflection potentials present the best estimates for $E^{(0)}$ from voltammograms showing irreversible behavior. Overall, differential analysis (needed for determining $E^{(i)}$) has the power to reveal subtle features of voltammograms (Figures 3, 6, 8). This property of differential

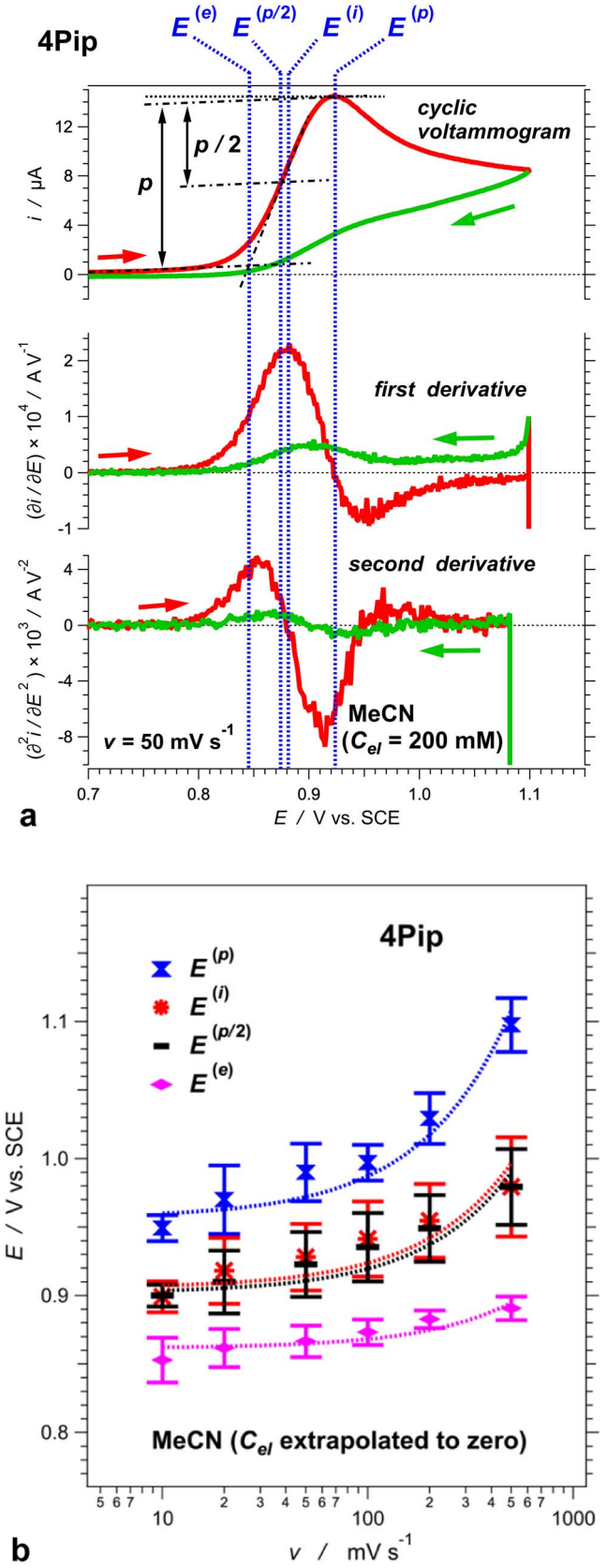

Figure 8. Electrochemical properties of 4Pip. (a) Cyclic voltammogram, along with its first and second derivative, of 4Pip (1 mM) recorded at 50 mV s^{-1} in the presence of 200 mM $N(C_4H_9)_4PF_6$. The different potentials obtainable from the anodic wave are designated. (b) Dependence of the different potentials of 4Pip on the scan rate. The potentials are obtained from extrapolation to zero concentration of $N(C_4H_9)_4PF_6$.

analysis, however, is also responsible for amplifying the inherent experimental noise. While lowering the analyte concentration is essential for reliability of the recorded voltammetric data (Figure 2a), it also decreases the signal-to-noise ratios. To address this challenge, we subject the first-derivatives curves to smoothing prior to the second numerical differentiation, as stated in the Experimental section. Limiting the span of shape smoothing to about 25 data points (at 1 mV per a data-point increment) ensures that the uncertainties in the obtained values for the potentials at the curve extrema are considerably smaller that the thermal energy, i.e., $<< Fk_BT$.

The differential nature of the analysis producing $E^{(i)}$, provides its most important advantage over $E^{(p/2)}$. The half-peak potential, $E^{(p/2)}$, depends only on three points: the baseline current, the peak current and the potential on the curve at the midpoint between these currents. Thus, $E^{(p/2)}$ cannot account for complex shapes of voltammogramic waves. Conversely, differential analysis can reveal shoulders and overlapping waves, producing multiple inflection points. This feature can prove invaluable for the analysis of: (1) multi-electron processes; and (2) samples comprising a mixture of conformers or aggregates exhibiting close, but different, reduction potentials. For example, when the potentials of two sequential electron-transfer steps are relatively close, the voltammogramic waves can appear broad but they cannot be discerned from those of single-step multi-electron processes.[13,15] Increasing the difference between the potentials of sequential reduction or oxidation steps, first broadens the waves, then leads to the appearance of a shoulder and finally results in two distinct peaks. Differential analysis can prove invaluable for analysis of such complex shapes and allow for selective evaluation of $E^{(i)}$ of the first step, for example.

In addition to the scan rates and other experimental settings, the shapes of voltammograms depends on: (1) the rates of interfacial electron transfer, characterized with $k^{(0)}$; (2) the rates of diffusion of the reduced and oxidized forms of the analyte, D_{red} and D_{ox}; (3) the charge transfer coefficient, α; and (4) the rates of degradation or other chemical transformation that depletes the electrochemically formed species, as characterized with k, for example. Different $k^{(0)}$, k, D_{ox}, D_{red}, and α result in voltammograms with different shapes where $E^{(p)}$ varies the most.[11] While $E^{(e)}$ and $E^{(i)}$ appear to be least susceptible to these multiparameter variations, $E^{(e)}$ inherently always underestimates and overestimates $E^{(0)}$ of oxidation and reduction, respectively. Therefore, $E^{(i)}$ is the closest estimate of $E^{(0)}$ that is easy to obtained from voltammograms manifesting irreversible behavior.

Conclusions

The half-wave potential, which are readily obtainable from cyclic voltammograms, are by far the best representation for $E^{(0)}$ even in cases manifesting partial irreversibility due to slow decomposition of the produced species. Conversely, all evidence suggest that when $E^{(1/2)}$ is not attainable due to complete chemical irreversibility, the inflection potentials and the half-peak potentials provide the best estimates for $E^{(0)}$, for moderate scan rates, e.g., 100 – 500 mV s^{-1}. While in many cases $E^{(i)}$ and $E^{(p/2)}$ perform almost the same, the values of $E^{(i)}$ tend to be inherently closer to $E^{(1/2)}$ than those of $E^{(p/2)}$. This report provides an important foundation and key evidence for transforming widely accepted practices of analyzing electrochemical findings in order to improve and broaden their utility.

Acknowledgments

We extend our gratitude to the U.S.A. National Science Foundation for supporting this research (grants CHE 1465284 and CHE 1800602).

ORCID

Valentine I. Vullev https://orcid.org/0000-0002-3416-9686

References

1. C. Costentin, J.-M. Saveant, and C. Tard, *ACS Energy Lett.*, **3**, 695 (2018).
2. N. Arshad and S. I. Farooqi, *Appl. Biochem. Biotechnol.*, **186**, 1090 (2018).
3. J. B. Derr, J. Tamayo, E. M. Espinoza, J. A. Clark, and V. I. Vullev, *Can. J. Chem.*, **96**, 843 (2018).
4. A. J. Wierzba, A. Wincenciuk, M. Karczewski, V. I. Vullev, and D. Gryko, *Chem. Eur. J.*, **24**, 10344 (2018).
5. N. T. Rodeberg, S. G. Sandberg, J. A. Johnson, P. E. M. Phillips, and R. M. Wightman, *ACS Chem. Neurosci.*, **8**, 221 (2017).
6. F. Harnisch and S. Freguia, *Chem. Asian J.*, **7**, 466 (2012).
7. I. Hwang and K. Yong, *ChemElectroChem*, **2**, 634 (2015).
8. S. Gupta, M. R. Chatni, A. L. N. Rao, V. I. Vullev, L. V. Wang, and B. Anvari, *Nanoscale*, **5**, 1772 (2013).
9. C. E. Nebel, B. Rezek, D. Shin, and H. Watanabe, *Physica Status Solidi A*, **203**, 3273 (2006).
10. N. Armaroli, G. Accorsi, F. Song, A. Palkar, L. Echegoyen, D. Bonifazi, and F. Diederich, *ChemPhysChem*, **6**, 732 (2005).
11. D. A. C. Brownson et al., "Interpreting Electrochemistry" in *The Handbook of Graphene Electrochemistry*, D. A. C. Brownson and C. E. Banks Editors, p. 23, Springer-Verlag London Ltd. (2014).
12. B. J. Adesokan, X. Quan, A. Evgrafov, A. Heiskanen, A. Boisen, and M. P. Soerensen, *J. Electroanal. Chem.*, **763**, 141 (2016).
13. N. Elgrishi, K. J. Rountree, B. D. McCarthy, E. S. Rountree, T. T. Eisenhart, and J. L. Dempsey, *J. Chem. Educ.*, **95**, 197 (2018).
14. N. V. Rees and R. G. Compton, *Chem. Commun.*, **46**, 4238 (2010).
15. D. H. Evans, *Chem. Rev.*, **108**, 2113 (2008).
16. J. A. V. Butler, *Trans. Faraday Soc.*, **19**, 734 (1924).
17. T. Erdey-Gruz and M. Volmer, *Z. Physik. Chem.*, **150**, 203 (1930).
18. R. A. Marcus, *Angew. Chem. Inr. Ed. Engl.*, **32**, 1111 (1993).
19. C. Batchelor-McAuley, E. Kaetelhoen, E. O. Barnes, R. G. Compton, E. Laborda, and A. Molina, *ChemistryOpen*, **4**, 224 (2015).
20. E. Laborda, M. C. Henstridge, C. Batchelor-McAuley, and R. G. Compton, *Chem. Soc. Rev.*, **42**, 4894 (2013).
21. R. M. Wightman, M. R. Deakin, P. M. Kovach, W. G. Kuhr, and K. J. Stutts, *J. Electrochem. Soc.*, **131**, 1578 (1984).
22. E. M. Espinoza, J. M. Larsen, and V. I. Vullev, *J. Phys. Chem. Lett.*, **7**, 758 (2016).
23. A. Purc, E. M. Espinoza, R. Nazir, J. J. Romero, K. Skonieczny, A. Jeżewski, J. M. Larsen, D. T. Gryko, and V. I. Vullev, *J. Am. Chem. Soc.*, **138**, 12826 (2016).
24. E. M. Espinoza, J. M. Larsen-Clinton, M. Krzeszewski, N. Darabedian, G. D. T., and V. I. Vullev, *Pure Appl. Chem.*,**89**, 1777 (2017).
25. J. M. Larsen-Clinton, E. M. Espinoza, M. F. Mayther, J. Clark, C. Tao, D. Bao, C. M. Larino, M. Wurch, S. Lara, and V. I. Vullev, *Phys. Chem. Chem. Phys.*, **19**, 7871 (2017).
26. E. M. Espinoza, J. A. Clark, J. B. Derr, D. Bao, B. Georgieva, F. H. Quina, and V. I. Vullev, *ACS Omega*, **3**, 12857 (2018).
27. H. G. Ryu, M. F. Mayther, J. Tamayo, C. Azarias, E. M. Espinoza, M. Banasiewicz, L. G. Lukasiewicz, Y. M. Poronik, A. Jezewski, J. Clark, J. B. Derr, K. H. Ahn, D. T. Gryko, D. Jacquemin, and V. I. Vullev, *J. Phys. Chem. C*, **122**, 13424 (2018).
28. H. G. Roth, N. A. Romero, and D. A. Nicewicz, *Synlett*, **27**, 714 (2016).
29. M. S. Thomas, V. Nuñez, S. Upadhyayula, E. R. Zielins, D. Bao, J. M. Vasquez, B. Bahmani, and V. I. Vullev, *Langmuir*, **26**, 9756 (2010).
30. J. M. Larsen, E. M. Espinoza, J. D. Hartman, C.-K. Lin, M. Wurch, P. Maheshwari, R. K. Kaushal, M. J. Marsella, G. J. O. Beran, and V. I. Vullev, *Pure Appl. Chem.*, **87**, 779 (2015).
31. D. Bao, S. Upadhyayula, J. M. Larsen, B. Xia, B. Georgieva, V. Nunez, E. M. Espinoza, J. D. Hartman, M. Wurch, A. Chang, C.-K. Lin, J. Larkin, K. Vasquez, G. J. O. Beran, and V. I. Vullev, *J. Am. Chem. Soc.*, **136**, 12966 (2014).
32. D. Bao, B. Millare, W. Xia, B. G. Steyer, A. A. Gerasimenko, A. Ferreira, A. Contreras, and V. I. Vullev, *J. Phys. Chem. A*, **113**, 1259 (2009).
33. D. Bao, S. Ramu, A. Contreras, S. Upadhyayula, J. M. Vasquez, G. Beran, and V. I. Vullev, *J. Phys. Chem. B*, **114**, 14467 (2010).
34. E. T. S. G. da Silva, S. Miserere, L. T. Kubota, and A. Merkoci, *Anal. Chem.*, **86**, 10531 (2014).
35. A. A. G. F. Beati, R. M. Reis, R. S. Rocha, and M. R. V. Lanza, *Industr. Eng. Chem. Res.*, **51**, 5367 (2012).
36. M. Abdul Aziz, B.-K. Kim, M. Kim, S.-Y. Yang, H.-W. Lee, S. W. Han, Y. I. Kim, S. Jon, and H. Yang, *Electroanalysis*, **23**, 2042 (2011).
37. G. Jones II, X. Zhou, and V. I. Vullev, *Photochem. Photobiol. Sci.*, **2**, 1080 (2003).
38. M. Diaz-Gonzalez, C. Fernandez-Sanchez, and A. Costa-Garcia, *Electroanalysis*, **14**, 665 (2002).
39. G. Jones II and V. I. Vullev, *Org. Lett.*, **4**, 4001 (2002).
40. P. Hrncirova and F. Opekar, *Sens. Actuat. B*, **81**, 329 (2002).
41. V. I. Vullev and G. Jones, *Tetrahedr. Lett.*, **43**, 8611 (2002).
42. D. K. Lee, H. J. Lee, G. S. Cha, H. Nam, and K. J. Paeng, *J. Chromatogr. A*, **902**, 337 (2000).
43. G. Jones II, V. Vullev, E. H. Braswell, and D. Zhu, *J. Am. Chem. Soc.*, **122**, 388 (2000).
44. S. Taunier, C. Guery, and J. M. Tarascon, *Electrochim. Acta*, **44**, 3219 (1999).
45. C. D. T. Bratten, P. H. Cobbold, and J. M. Cooper, *Anal. Chem.*, **69**, 253 (1997).
46. G. Jones II, L. N. Lu, V. Vullev, D. Gosztola, S. Greenfield, and M. Wasielewski, *Bioorg. Med. Chem. Lett.*, **5**, 2385 (1995).
47. E. Halls Jonathan, A. Hernan-Gomez, D. Burrows Andrew, and F. Marken, *Dalton Transact.*, **41**, 1475 (2012).

48. Zheng, Evans, and Nelsen, *J. Org. Chem.*, **65**, 1793 (2000).
49. B. Bry and B. Tremillon, *J. Electroanal. Chem. Interfac. Electrochem.*, **46**, 71 (1973).
50. S. P. Gubin, S. A. Smirnova, L. I. Denisovich, and A. A. Lubovich, *J. Organometal. Chem.*, **30**, 243 (1971).
51. A. M. Bond, K. B. Oldham, and G. A. Snook, *Anal. Chem.*, **72**, 3492 (2000).
52. A. M. Bond, E. A. McLennan, R. S. Stojanovic, and F. G. Thomas, *Anal. Chem.*, **59**, 2853 (1987).
53. R. R. Gagne, C. A. Koval, and G. C. Lisensky, *Inorg. Chem.*, **19**, 2854 (1980).
54. S. Trasatti, *Pure Appl. Chem.*, **58**, 955 (1986).
55. W. M. Latimer, *J. Am. Chem. Soc.*, **76**, 1200 (1954).
56. J. M. Larsen, E. M. Espinoza, and V. I. Vullev, *J. Photon. Energy.*, **5**, 055598 (2015).
57. M. K. Ashraf, R. R. Pandey, R. K. Lake, B. Millare, A. A. Gerasimenko, D. Bao, and V. I. Vullev, *Biotechnol. Progr.*, **25**, 915 (2009).
58. V. I. Vullev, *J. Phys. Chem. Lett.*, **2**, 503 (2011).
59. B. Xia, D. Bao, S. Upadhyayula, G. Jones, and V. I. Vullev, *J. Org. Chem.*, **78**, 1994 (2013).
60. S. Upadhyayula, D. Bao, B. Millare, S. S. Sylvia, K. M. M. Habib, K. Ashraf, A. Ferreira, S. Bishop, R. Bonderer, S. Baqai, X. Jing, M. Penchev, M. Ozkan, C. S. Ozkan, R. K. Lake, and V. I. Vullev, *J. Phys. Chem. B*, **115**, 9473 (2011).
61. E. M. Espinoza, B. Xia, N. Darabedian, J. M. Larsen, V. Nunez, D. Bao, J. T. Mac, F. Botero, M. Wurch, F. Zhou, and V. I. Vullev, *Eur. J. Org. Chem.*, **2016**, 343 (2016).
62. M. Krzeszewski, E. M. Espinoza, C. Cervinka, J. B. Derr, J. A. Clark, D. Borchardt, G. J. O. Beran, D. T. Gryko, and V. I. Vullev, *Angew. Chem., Int. Ed.*, **57**, 12365 (2018).
63. O. Borodin, S.-D. Han, J. S. Daubert, D. M. Seo, S.-H. Yun, and W. A. Henderson, *J. Electrochem. Soc.*, **162**, A501 (2015).
64. M. Born, *Z. Phys.*, **1**, 45 (1920).
65. M. J. Bird, T. Iyoda, N. Bonura, J. Bakalis, A. J. Ledbetter, and J. R. Miller, *J. Electroanal. Chem.*, **804**, 107 (2017).
66. T. Kakiuchi, J. Noguchi, and M. Senda, *J. Electroanal. Chem.*, **327**, 63 (1992).
67. M. Rosenblum, J. O. Santer, and W. G. Howells, *J. Am. Chem. Soc.*, **85**, 1450 (1963).
68. A. F. Cunningham Jr., *J. Am. Chem. Soc.*, **113**, 4864 (1991).
69. M. J. Mayor-Lopez, J. Weber, B. Mannfors, and A. F. Cunningham Jr., *Organometallics*, **17**, 4983 (1998).
70. A. H. Ilkhechi, J. M. Mercero, I. Silanes, M. Bolte, M. Scheibitz, H.-W. Lerner, J. M. Ugalde, and M. Wagner, *J. Am. Chem. Soc.*, **127**, 10656 (2005).
71. J. Rodríguez-Otero, E. M. Cabaleiro-Lago, Á. Peña-Gallego, and M. Merced Montero-Campillo, *Tetrahedron*, **65**, 2368 (2009).
72. A. Irigoras, J. M. Mercero, I. Silanes, and J. M. Ugalde, *J. Am. Chem. Soc.*, **123**, 5040 (2001).
73. M. Scheibitz, R. F. Winter, M. Bolte, H.-W. Lerner, and M. Wagner, *Angew. Chem. Int. Ed.*, **42**, 924 (2003).
74. N. Grover, M. Sankar, Y. Song, and K. M. Kadish, *Inorg. Chem.*, **55**, 584 (2016).
75. M. Boulkroune, L. Ignatovich, V. Muravenko, J. Spura, A. Chibani, and V. Jouikov, *Chem. Heterocyclic Compounds*, **49**, 1579 (2014).
76. S. Zhu, Q. Song, S. Zhang, and Y. Ding, *J. Molecul. Struct.*, **1035**, 224 (2013).
77. T. Fujimoto, M. M. Matsushita, and K. Awaga, *J. Phys. Chem. C*, **117**, 5552 (2013).
78. M. Schmittel, Q. Shu, and M. E. Cinar, *Dalton Transact.*, **41**, 6064 (2012).
79. K. R. Edelman and B. J. Holliday, *Inorg. Chem.*, **49**, 6787 (2010).
80. A. A. Popov, I. E. Kareev, N. B. Shustova, E. B. Stukalin, S. F. Lebedkin, K. Seppelt, S. H. Strauss, O. V. Boltalina, and L. Dunsch, *J. Am. Chem. Soc.*, **129**, 11551 (2007).
81. G. V. Loukova and V. V. Strelets, *Russ. Chem. Bull.*, **49**, 1037 (2000).